Advanced Lab Course

Quantum Information Using Nitrogen-Vacancy Centers in Diamond*

Authors: Eduard Koller (03702415)
Michael Labenbacher (03697519)
Daniel Haag (03697076)

Group: 17

Supervisor: Amawi Mohammad

Date of lab course: Friday 15th November, 2019
Date of submission: Tuesday 26th November, 2019

*corrected version, last updated Saturday 11th January, 2020

Contents

1. Introduction

This lab course will demonstrate basic concepts of quantum information. Therefore qubit initialization, simple readout and pulsed measurement protocols are tested on nitrogen-vacancy centers in diamond. As a model, a spin in a constant magnetic field is taken as a basis, and the state is manipulated with a microwave field.

2. Theoretical Background

2.1. Electron Paramagnetic Resonance (EPR)

The spin of an electron subjected to a constant magnetic field, $\mathbf{B}_0 = B_0\hat{e}_z$, precesses around the $\mathbf{B}_0$ with the Larmor frequency, defined by

$$\hbar\omega_\mathrm{L} = g_\mathrm{e}\mu_\mathrm{B}B_0, \tag{1}$$

with g_e the Landé g-factor of the electron, μ_B the Bohr magneton and $\hbar$ the reduced Planck constant. Depending on the spin eigenvalue, $\mathbf{B}_0$ either increases or decreases the energy of the electron. The difference in energy is $g_\mathrm{e}\mu_\mathrm{B}B_0$.

In this lab course the spin is also subjected to a weak driving magnetic field

$$\mathbf{B}_1 = B_1\big(\sin(\omega_\mathrm{ph}t)\hat{e}_x + \cos(\omega_\mathrm{ph}t)\hat{e}_y\big). \tag{2}$$

If the photon energy $\hbar\omega_\mathrm{ph}$ matches the energy splitting

$$\omega_\mathrm{ph} = \omega_\mathrm{L}, \tag{3}$$

resulting from the constant magnetic field, the photon can be absorbed and causes the electron state to change between $m_\mathrm{S} = 1$ and -1. This is given by the time evolution of the state vector, described in sec. 2.2, and depends on the duration the magnetic field $\mathbf{B}_1$ is switched on.

2.2. Rotating Reference Frame

In this lab course, the reference frame precesses around the z-axis with the frequency ω_ph. Therefore, under condition (3), $\mathbf{B}_1$ is a constant vector in the rotating frame. For the sake of simplicity, $\mathbf{B}_1 = B_1\hat{e}_x$ in this lab course.

The spin now precesses around the z-axis with the detuning frequency,

$$\Delta\omega = \omega_\mathrm{ph} - \omega_\mathrm{L}. \tag{4}$$

A spin state $|\psi\rangle$ is represented by the Bloch vector

$$\boldsymbol{\psi} = \begin{pmatrix} \sin(\theta)\cos(\phi) \\ \sin(\theta)\sin(\phi) \\ \cos(\theta) \end{pmatrix}, \tag{5}$$

where θ is the angle measured from the z-axis and

$$\phi = \Delta\omega t \tag{6}$$

is the angle measured from the x-axis in the x-y-plane.

It can be shown that in the rotating frame the spin rotates around an effective magnetic field $\mathbf{B}_{\text{eff}}$, described by

$$\frac{\mathrm{d}\boldsymbol{\psi}}{\mathrm{d}t} = \gamma \cdot \boldsymbol{\psi} \times \mathbf{B}_{\text{eff}}, \qquad \mathbf{B}_{\text{eff}} = B_1 \hat{e}_x + \frac{\Delta\omega}{\gamma}\hat{e}_z, \tag{7}$$

where $\gamma = g_e \mu_{\text{B}}/\hbar$ is the gyromagnetic ratio. [1] In this lab course $\boldsymbol{\psi}$ therefore rotates parallel to the y-z-plane. The speed of that rotation depends on B_1.

2.3. The Nitrogen-Vacancy Center

In this lab course, the described theory will be applied to the nitrogen-vacancy center, a lattice defect, in diamond. These consists of a nitrogen atom and a vacancy. It replaces two nearest neighboring carbon atoms along the [111]-axis (or $[\bar{1}\bar{1}1]$, $[1\bar{1}\bar{1}]$, $[\bar{1}1\bar{1}]$).

The energy level scheme for this spin system is given in fig. 1. The states discussed in the following are the ground state triplet $|\text{g}\rangle$, the excited state triplet $|\text{e}\rangle$ and furthermore the shelving state $|\text{s}\rangle$. Both $|\text{g}\rangle$ and $|\text{e}\rangle$ split into $m_{\text{S}} = 0$ and $m_{\text{S}} = \pm 1$. [2]

Without the presence of an external magnetic field, states with $m_{\text{S}} = \pm 1$ are degenerate[1]. Between $m_{\text{S}} = 0$ and $m_{\text{S}} = \pm 1$, there is, however, a difference in energy. That is referred to as zero field splitting. A transition between $m_{\text{S}} = 0$ and $m_{\text{S}} = \pm 1$ requires photons with a frequency of $D_{|\text{g}\rangle} = 2.87\,\text{GHz}$ or $D_{|\text{e}\rangle} = 1.42\,\text{GHz}$. In this lab course, those photons are emitted by a continuous wave microwave generator (MW).

If the system is subjected to a constant magnetic field $\mathbf{B}_0$, a transition between $m_{\text{S}} = 0$ and $m_{\text{S}} = \pm 1$ of $|\text{g}\rangle$ requires photons with a frequency of

$$\omega_{\text{mw}} = D_{|\text{g}\rangle} \pm \gamma_{\text{NV}} B_0, \tag{8}$$

where $\gamma_{\text{NV}} = 28\,\text{GHz/T}$ is the gyromagnetic ratio of the nitrogen-vacancy center. [2]

An absorption between $|\text{g}\rangle$ and $|\text{e}\rangle$ requires photons with a wavelength of $\lambda = 520\,\text{nm}$. In this lab course, those photons are emitted by a laser.

$|\text{e}, m_{\text{S}} = 0\rangle$ decays to $|\text{g}, m_{\text{S}} = 0\rangle$ by emitting a red photon with a wavelength of $\lambda = 638\,\text{nm}$. [2] In addition to an analogous decay, $|\text{e}, m_{\text{S}} = \pm 1\rangle$ decays with a substantial probability via an alternative pathway, over the shelving state $|\text{s}\rangle$, to $|\text{g}, m_{\text{S}} = 0\rangle$ without emitting a red photon and a relatively high relaxation time of $\sim 300\,\text{ns}$. [2] Therefore the laser can be used to initialize the spins in $|g, m_{\text{S}} = 0\rangle$. This effect also makes it possible to read out the spin state. When all nitrogen-vacancy centers are in $m_{\text{S}} = 0$, the intensity of the emitted photons is maximal. Thus, an NV ensemble with more population in $m_{\text{S}} = \pm 1$ has a less bright fluorescence than one with more population in $m_{\text{S}} = 0$.

3. Experimental Setup

The diamond, an antenna, a camera with an optical filter and the laser are all mounted in a box. The antenna emits the pulsed microwaves generated by the continuous wave microwave generator modulated by a field-programmable gate array (FPGA). The camera registers the red photons emitted by decays. The laser, the switch and the microwave generator are connected to a computer. The signal from the camera, after being amplified, is received by that computer. After the first measurement, a magnet is mounted in the box. Its magnetic field is $\mathbf{B}_0$.

In a program, all systems are calibrated. The measurements are conducted with the same program. Each measurement consists of a sequence of commands. The sequence is executed a given amount of times. Depending on the measurement, either the frequency of the microwave generator or a time period is increased with each cycle.

[1] Each of these state is further split by higher-order interactions, but this will be neglected in the lab course.

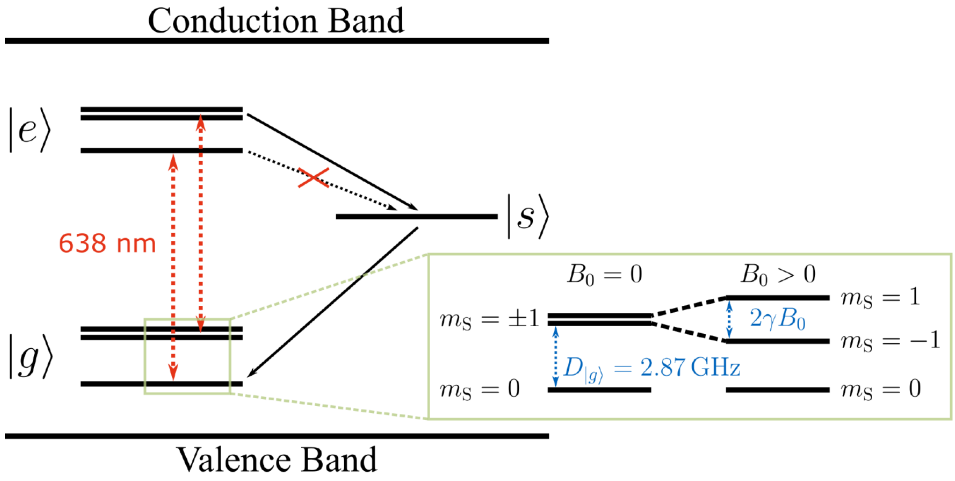

Figure 1: Energy level scheme of the NV^- center in diamond. [2]

For all measurements, the first command of the sequence is a laser pulse of 300 ns. This not only initializes the nitrogen-vacancy centers into $|m_S = 0\rangle$ of $|g\rangle$ but also allows the camera to register the previous cycle (readout of the spin state). This command is followed by a waiting period, which must be greater than the relaxation time of the shelving state and is therefore also a part of the initialization, and this also ensures that the laser and the microwave generator are not active at the same time. The following commands depend on the measurement and are described in the respective sections.

Before each measurement, the laser is pulsed for a short period of time allowing it to warm up.

4. Measurement of the Zero Field Splitting

In the first part, the zero field splitting $D_{|g\rangle}$ shall be measured. This is done by the following sequence, whereby the initialization and readout is done at the same time:

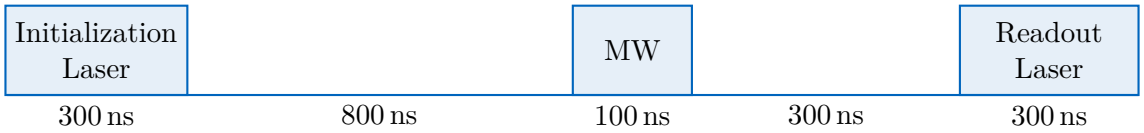

The frequency of the microwaves increases from 2 600 MHz to 3 000 MHz with a step size of 5 MHz and 4 repetitions.

The laser was previously heated up (pulsed). In order to minimize the influence of the temperature, due to further heating up processes, and intensity dependence of the laser, the data were fitted (and then corrected) with a (2nd order) polynomial fit outside the range of the minimum (2 850 MHz to 2 900 MHz), the result is shown in fig. 2.

The sudden and obvious dip in fig. 2 in intensity of about 1.75 % is at a frequency of (2 872 ± 9) MHz. This refers to the resonance frequency $D_{|g\rangle}$ of this transition. The readout accuracy can be estimated from the plot from the intensity distribution at non-resonant microwave frequency and is approximately less than 0.5 %.

For the width of the minimum, in addition to a certain frequency uncertainty, one must recall that diamond is a complex many-particle quantum system and the considered spin system is not one of isolated spins.

The theoretical value given in [2] is $D_{|g\rangle} = 2.87$ GHz. That matches the experimental value sufficiently. With this setup only the zero field splitting of the ground state can be measured,

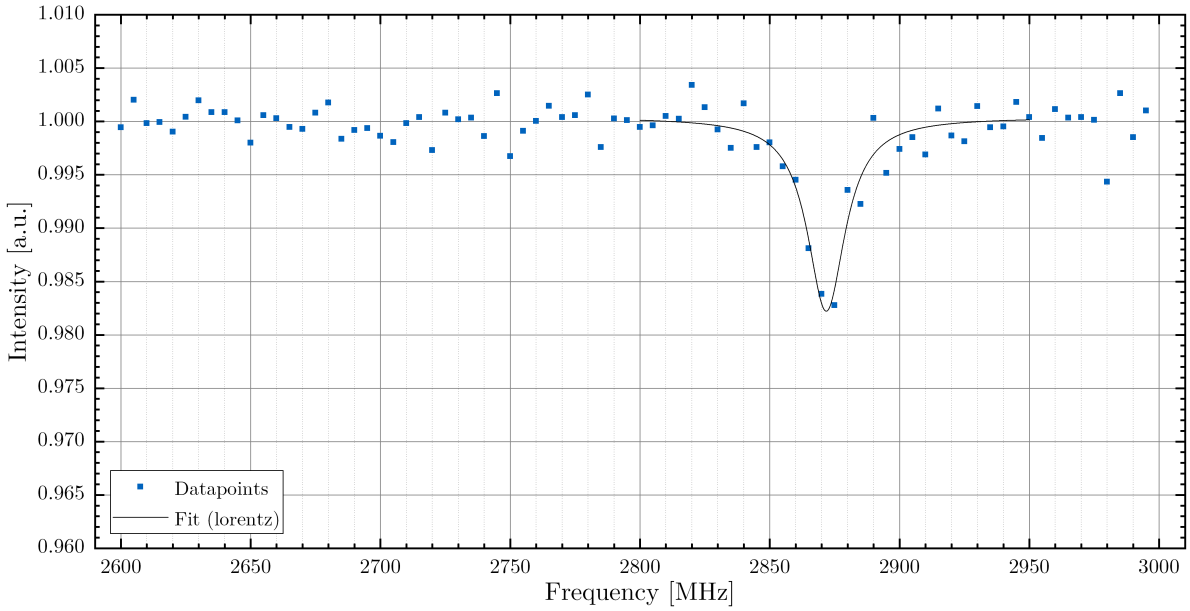

Figure 2: Zero field splitting. NV fluorescence as a function of the MW frequency. The minimum is the spin resonance, in which a ratio of the excited states can relax over the shelving state without radiation.

because the excited state is not stable and therefore a initialization in $m_S = 0$ of $|e\rangle$ is not possible.

5. Measurement of the Zeeman Splitting

In this part the Zeeman splitting between $|g, m_S = 1\rangle$ and $|g, m_S = -1\rangle$ should be measured. For this a cubic shaped permanent magnet is mounted near the diamond, whereby, due to the small size of the diamond, we assume the field is constant, for more see sec. 8. As mentioned in sec. 3 the same sequence as in the previous section 4 is used.

In addition to the magnetic field (zero field splitting) in which the spin is located, the external field is added, whereby only the component parallel to the old quantization axis matters. As mentioned in sec. 2.3 the nitrogen-vacancy center in diamond can be oriented in four directions and thus we expect up to four symmetric splits and therefore a maximum of eight minima in the emission spectrum. The splitting depends on the projection of the constant magnetic on the axis of the NV center. However, these splits can also be close together or out of the frequency range of the measurement and then it is not possible to dissolve or see all minima.

The laser was previously heated up (pulsed) and the frequency of the microwaves increases from 2 600 MHz to 3 000 MHz with a step size of 1 MHz and 10 repetitions. The data, after being fitted as seen in sec. 4, is shown in fig. 3.

The measurement, plotted in fig. 3, shows six resonances. The symmetry axis should be at the frequency of the zero field splitting at $(2\,872 \pm 9)$ MHz, but the three resonances at high frequencies are about 2 878 MHz symmetrical to the resonances at low frequencies. This is inside the tolerance range, but can also indicate a small asymmetry in the g-factor.

The difference in the decrease in intensity at the resonances can perhaps be explained by the fact that three defect orientations each have a resonance frequency with a not negligible width, already explained in sec. 2, are close to one another.

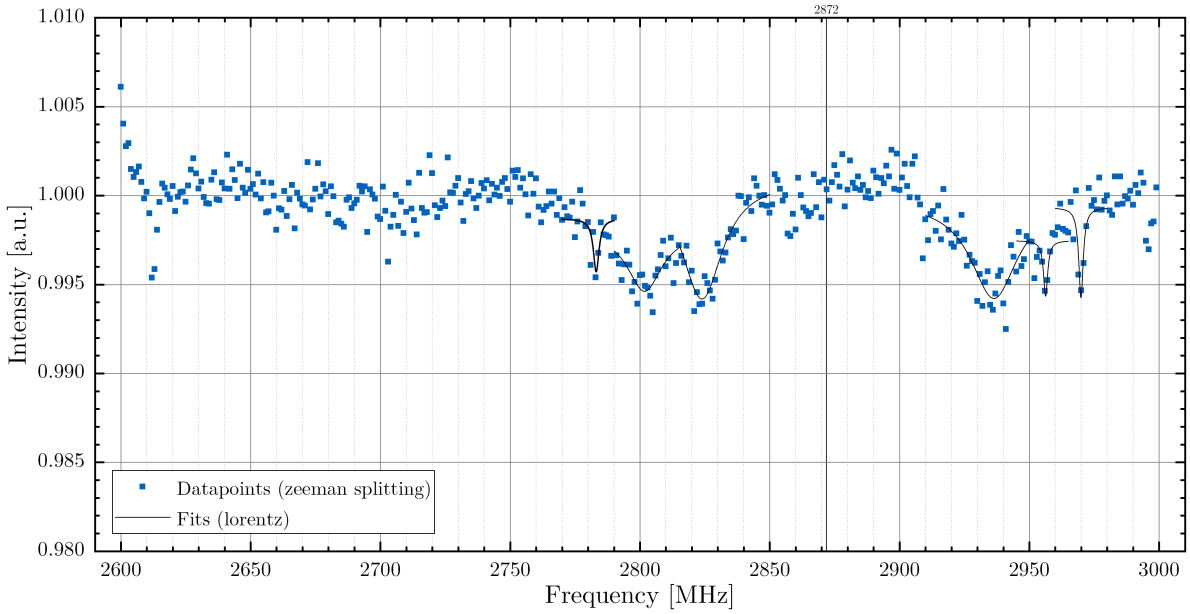

Figure 3: Zeeman splitting due to an external constant magnetic field. A nearly symmetrically distribution, around the resonance frequency of the zero field splitting, can be detected. For each different oriented NV centers a pair of resonance frequencies can be assigned. Due to symmetry three resonances can be identified at $(2\,783 \pm 5)$ MHz, $(2\,800 \pm 5)$ MHz and $(2\,824 \pm 5)$ MHz, in the lower frequency range, and three at $(2\,970 \pm 5)$ MHz, $(2\,956 \pm 5)$ MHz and $(2\,936 \pm 5)$ MHz, in the upper range. Furthermore a drop in intensity at approx. 2 613 MHz can be detected, which can belong to the last different oriented NV centers, the corresponding drop at high frequencies should therefore be outside of the observed measuring range at approx. $(3\,133 \pm 5)$ MHz.

6. Determination of the π-Pulse

If an oscillating magnetic field $\mathbf{B}_1$ matches the Larmor frequency of a two level spin system, the time evolution can be visualized on the Bloch sphere. In the rotating reference frame, where $\mathbf{B}_1$ is constant, the spin then rotates vertically around this magnetic field and performs a circular motion. If the spin is initialized in the state $m_S = 0$, the z-component of the spin oscillates between $m_S = 0$ and $m_S = \pm 1$ (the sign follows from the chosen frequency of the Zeeman splitting, see sec. 5), whereby in this lab course z is the quantization axis of the external constant magnetic field $\mathbf{B}_0$, responsible for the Zeeman splitting.

To get spins from the ground state as efficiently as possible into the excited state, the duration of the oscillating magnetic field must be chosen so that the spin performs exactly half a rotation. This corresponds to half the period of the Rabi oscillation and such a pulse is called a π-pulse.

To determinate the duration of a π-pulse, which is needed in sec. 7 and 8, the Rabi sequence is used:

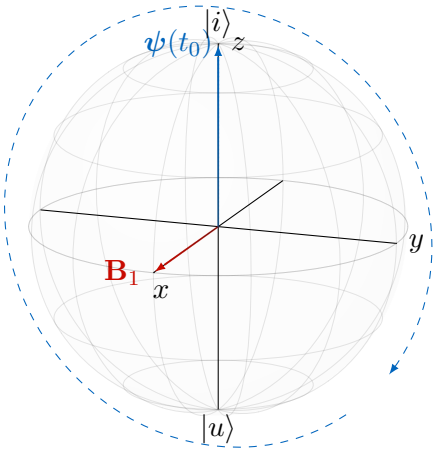

Figure 4: Bloch sphere for the evolution of the spin visualized in the rotating frame under the influence of the MW in x-direction. $|i\rangle$ represents the initialized state and $|u\rangle$ refers to the chosen excited state with $m_S = 1$ or $m_S = -1$.

As in the previous sections initialization in the ground state $|i\rangle = |g, m_S = 0\rangle$ and readout are done at the same time. The variable in this sequence is the MW duration t from 10 ns to 200 ns in 4.5 ns-steps and 10 repetitions. The microwave frequency was set to 2 825 MHz, one of the NV spin resonance frequencies, estimated during the lab course, in sec. 5.

The measurement values are shown in fig. 5. The maximum at the beginning results from the fact that no spin transition is driven. A possible oscillation is only slightly visible. For further measurements a π-pulse of 60 ns was chosen, due to the fact that it is the first recognizable minima (green) in fig. 5, determined during the lab course, and it is roughly within the expected measuring range, given by the tutor.

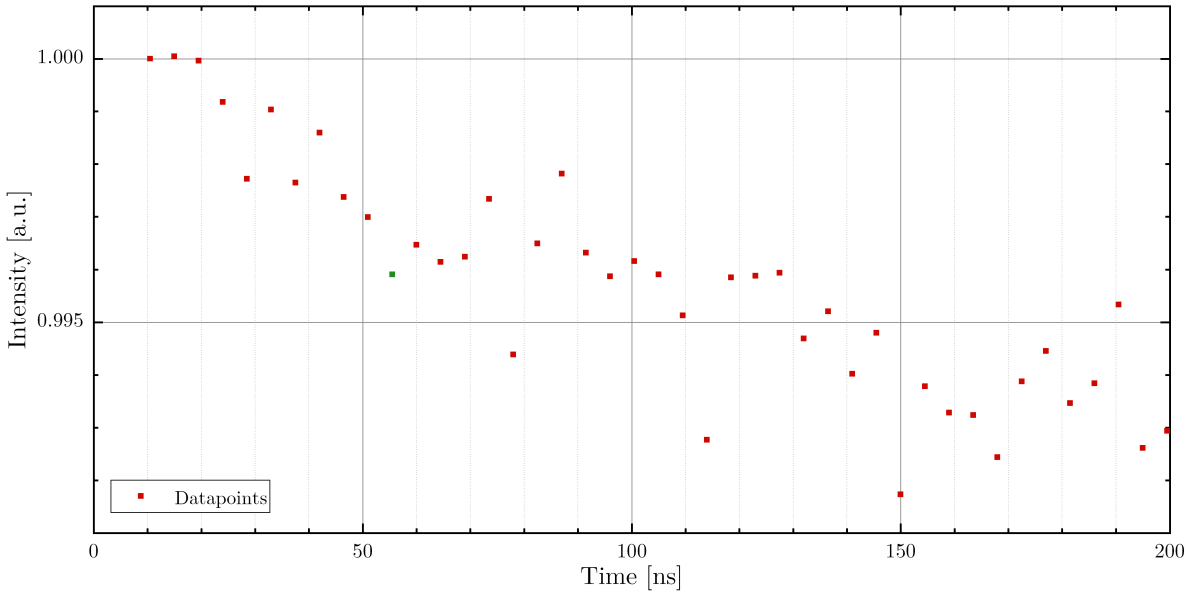

Figure 5: Rabi oscillation. NV fluorescence as a function of the MW pulse duration t. The oscillations are hardly visible. However considering the approximate readout accuracy of max. 0.5 % determined in sec. 4, the first minimum can be estimated at (56 ± 10) ns. Also at approximately twice the time a minimum at (114 ± 10) ns can be identified.

After approximately 140 ns the measured values in fig. 5 seems to be entirely random. There are several reasons for the decay of the Rabi oscillations. First the microwave frequency does not exactly match the Larmor frequency of the spin system and this increasingly detunes the rotating reference frame and the driving magnetic field. As mentioned in the previous section the spin system is not an isolated one, as assumed in the derivation, see sec. 2. Therefore one must also consider interactions with the surroundings, for example there are also spin-spin interactions, and in the long term allowing the spin populations to equilibrate.

7. Ramsey Sequence

In the case $\Delta\omega = \omega_{ph} - \omega_L \neq 0$, the spin precesses with the detuning frequency around the z-axis and the representing Bloch vector suffers a change by an angle ϕ in the x-y-plane according to equ. (6) where $t = \tau$ is the (pulse-)free evolution time. The detuning frequency can be measured with the Ramsey sequence:

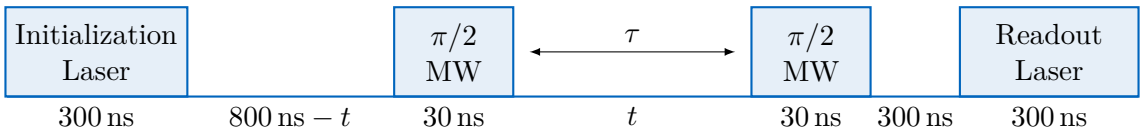

As always initialization and readout are done at the same time, the variable is the waiting time $t = \tau$ which increases from 10 ns to 200 ns with a step size of 4.5 ns and 10 repetitions. The microwave frequency was set to the same resonance frequency of 2 825 MHz as in sec. 6.

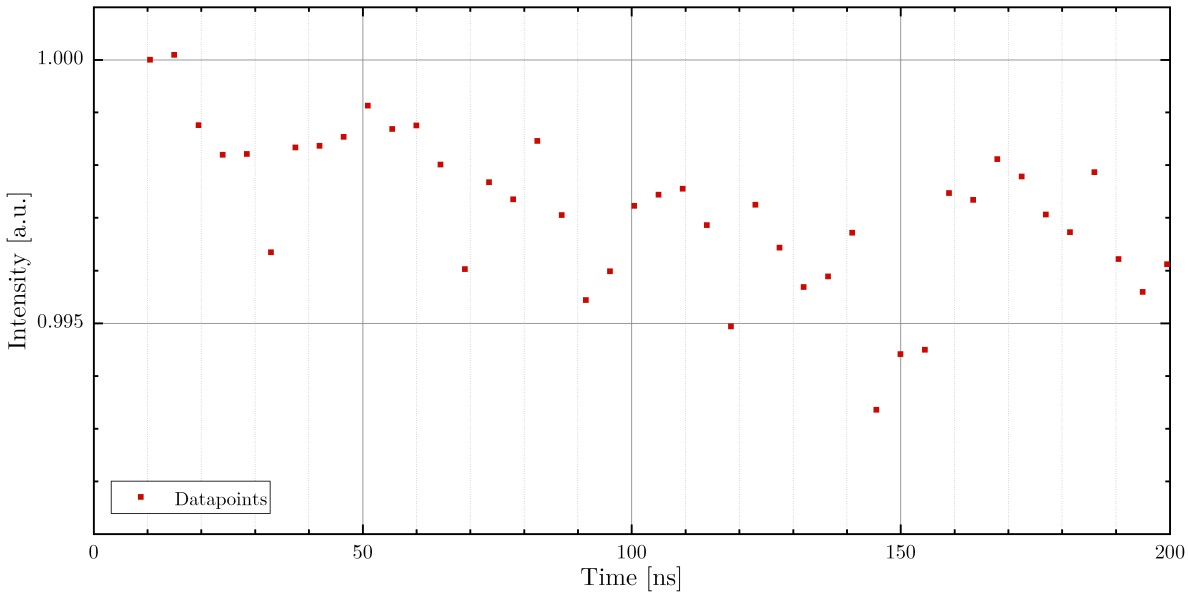

Figure 6: Ramsey oscillation. NV fluorescence as a function of the pulse-free evolution time t. The oscillations are hardly visible and taking the approximated readout accuracy of 0.5 % in sec. 4 the fluctuations are too small.

The resulting measurement graph 6 indicates an oscillation of the z-component, but with the approximated readout accuracy one can not determine the detuning frequency with this measurement.

An explanation for the obtained result would be, that with $\frac{2\pi}{\tau_{2\pi}} = \Delta\omega \ll \Omega = \frac{2\pi}{t_{2\pi}}$ the chosen maximum waiting time of 200 ns, compared to the determined π-pulse with $t_{2\pi} = 120$ ns in sec. 6, is far to small.

8. Record of an Echo Revival

The last sequence to be investigated can be used to measure the spin-spin relaxation time or to detect magnetic signals with a certain frequency (, whereby in this lab course an echo revival is recorded). For an explanation one can use the Bloch sphere and has to consider an ensemble of spin systems. First all spins are initialized in the ground state ($|i\rangle$, top of the Bloch sphere, see fig. 4), secondly rotated via a $\pi/2$-pulse, then all spins are directed horizontally in the same direction. Theoretically if the constant magnetic field $\mathbf{B}_0$ is the same for all spins, these would precess around the z-axis with the same detuning frequency. But the magnetic field from the cubic magnet is not spatially constant and each spin of the ensemble precesses around the z-axis with its local detuning frequency. After the pulse-free evolution time τ_1 a π-pulse is used to invert all spin directions. After the same time τ_2, the variable in this sequence, passes, the signal should be corrected and a $\pi/2$-pulse rotates the spins back onto the z-axis for readout.

On this basis this technique allows the elimination of these inhomogeneities and thus makes an assessment of further deviations, such as spin-spin interactions.

To record an echo revival the Hahn sequence is used:

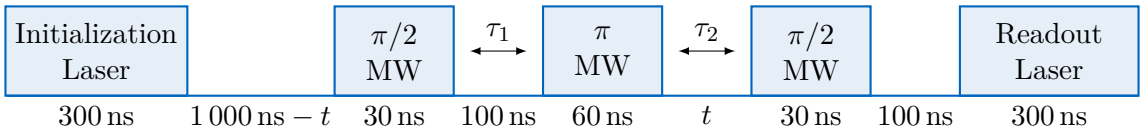

As always initialization and readout are done at the same time, the first pulse-free evolution time was constant $\tau_1 = 100\,\text{ns}$, the variable is the second time $t = \tau_2$ which increases from 10 ns to 200 ns with a step size of 4.5 ns and 4 repetitions. The microwave frequency was set to the same resonance frequency of 2 825 MHz as in sec. 6.

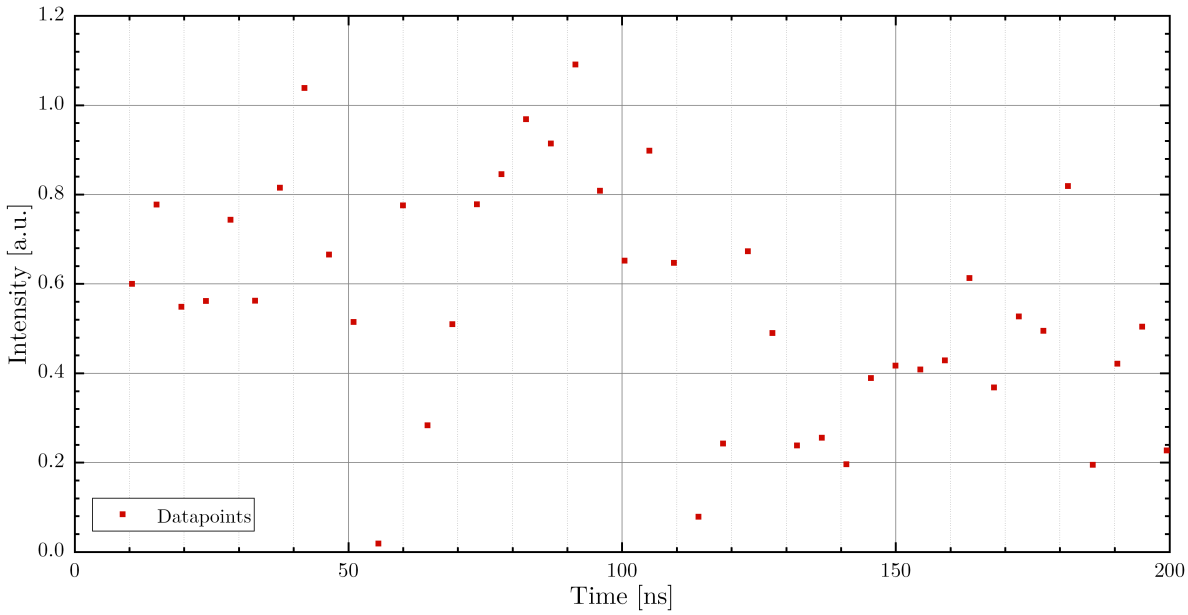

Figure 7: Echo revival. NV fluorescence as a function of the second pulse-free waiting time τ_2. Despite of high fluctuations, an increase near 100 ns can be detected.

The results are shown in fig. 7. From theory one would expect a Gaussian function around $\tau_1 = 100\,\text{ns}$, maximal intensity with matching precession times, because the inhomogeneities, caused by the spatially varying resonance condition, are then corrected away.

Since the Rabi oscillation in sec. 6 could only be measured vaguely, this measurement also implies a high error, since it is based on the π-pulse. A tendency towards the expected value of 100 ns, where the mean intensity is slightly increased, can nevertheless be seen in fig. 7.

If both free evolution times are equal $\tau = \tau_1 = \tau_2$ and used as a variable of the sequence, this creates a detector for signals with frequency near $f = \frac{1}{2\tau}$.

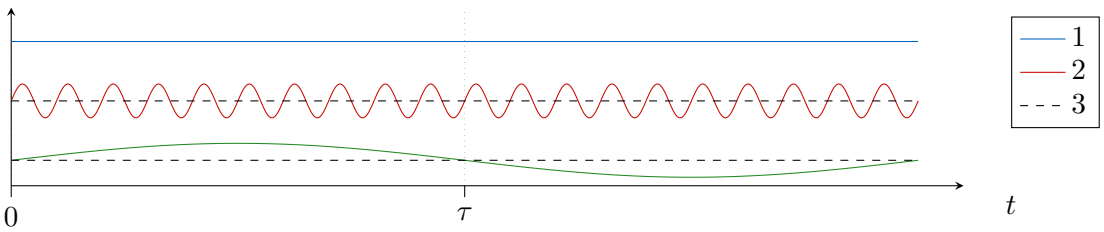

Figure 8: Simple diagram for the explanation to detect signals with a Hahn sequence.

Explanation (cases/color due to fig. 8): For the sake of simplicity neglect the duration of the π-pulse. In the first case (blue) consider a constant signal, then one will measure a maximal

intensity due to matching precession times, as described in this section 8. Secondly (red) consider high frequencies. The spins oscillate strongly around the z-axis and on average the detuning is nearly zero, thus one will also measure maximal intensity. A minimum in intensity will be measured, if the frequency reaches $f = \frac{1}{2\tau}$ (green), because after the π-pulse (invertation of all spin directions) the spins keep drifting further apart.

A. Bibliography

[1] M.A. Bernstein, K.F. King, and X.J. Zhou. *Handbook of MRI Pulse Sequences*. Elsevier Science, 2004. ISBN: 9780080533124 (cit. on p. 2).

[2] Georg Braunbeck. *Quantum Information Using Nitrogen-Vacancy Centers In Diamond*. 2018. URL: https://www.ph.tum.de/academics/org/labs/fopra/docs/userguide-15.en.pdf (visited on November 16, 2019) (cit. on pp. 2–3).

B. List of Figures